Finite element dq-model for MTPA flux control of Synchronous Reluctance Motor (SynRM)

Romain Delpoux, Thomas Huguet, Federico Bribiesca Argomedo, Loïc Queval, Jean-Yves Gauthier, Zohra Kader

Finite element dq-model for MTPA flux control of Synchronous Reluctance Motor (SynRM)

Romain Delpoux
Univ Lyon, INSA Lyon, Université Claude Bernard Lyon 1, Ecole Centrale de Lyon CNRS, Ampère, UMR5005
Villeurbanne, France
romain.delpoux@insa-lyon.fr

Thomas Huguet
LAPLACE
Univ Toulouse, CNRS, INPT, UPS
Toulouse, France
thomas.huguet@toulouse-inp.fr

Federico Bribiesca Argomedo
Univ Lyon, INSA Lyon, Université Claude Bernard Lyon 1, Ecole Centrale de Lyon CNRS, Ampère, UMR5005
Villeurbanne, France
federico.bribiesca-argomedo@insa-lyon.fr

Loïc Queval
GeePs
CentraleSupélec, University of Paris-Saclay
Paris, France
loic.queval@centralesupelec.fr

Jean-Yves Gauthier
Univ Lyon, INSA Lyon, Université Claude Bernard Lyon 1, Ecole Centrale de Lyon CNRS, Ampère, UMR5005
Villeurbanne, France
jean-yves.gauthier@insa-lyon.fr

Zohra Kader
LAPLACE
Univ Toulouse, CNRS, INPT, UPS
Toulouse, France
zohra.kader@laplace.univ-tlse.fr

***Abstract*—This article focuses on the modelling of SynRM including magnetic saturation and cross-saturation to obtain accurate dynamic simulations from models obtained by Finite Element Analysis (FEA). It is shown here that in the presence of nonlinear magnetic materials, the use of flux instead of current is of interest for both simulation and control design. From this observation, dynamic flux simulation model is obtained. The accuracy of the modelling is illustrated though the design of a Maximum Torque Per Ampere (MTPA) based flux control. Simulation results, close to the real SynRM obtained from FEA are conducted to validate the development and its practical usefulness.**

***Index Terms*—MTPA, flux control, FEA, dynamic model.**

I. Introduction

Permanent Magnet Synchronous Motors (PMSM), using rare-earth, are considered as the main candidate in most industrial applications due to their high performance. While these machines notably make it possible to offer vehicles that do not emit exhaust fumes and therefore reduce CO_2 emissions, environmental impacts of rare earth materials and supply risks, e.g. restricted access and price volatility, impacts their cost [13], [16]. The development of applications using rare-earth-free motors is today a strategic priority. In this context, SynRM technology gains more and more interest since a few years and becomes a serious competitor [8], [12]. Due to technical advances in computer science, electronics and power electronics, these machines seriously compete with asynchronous machines in terms of efficiency. New designs also continually improve them [3], these machines are now tending to compete with the PMSM [5] in various industrial applications [2], [11], due to increased efficiency and reduced weight [17]. In summary SynRM contributes towards more simple, resilient and robust electric motor to provide a credible ecological alternative to permanent magnet synchronous motors.

To become even more competitive, control algorithm improvement for these machines is a challenge. Indeed, under rated condition magnetic flux saturation occurs heavily, causing large nonlinearities [12]. Maximum Torque Per Ampere (MTPA) control is important to optimize energy efficiency of the motor. Recently, MTPA control for SynRM and interior permanent magnet motor drives has received a lot of attention as the recent literature review [18] can attest. In this article it is clearly stated that the presence of magnetic nonlinearities such as saturation and cross saturation makes the use of the notion of inductance complex, due to the difficulties about the precise knowledge of the differential inductances which intervene. The development of MTPA using apparent and differential inductances was developed in [6]. These nonlinearities make Look Up Table (LUT) based solutions the most common in the scientific literature [7], [9], where LUT provides current controller references. Since inductances are nonlinear, it seems interesting to focus on the flux rather than on current and thus to get rid of the problems of differential inductances. While flux is difficult to measure, it is often obtained from LUTs as function of current. Flux controller for SynRM was notably proposed for SynRM in [10], [19] using classical linear controller. Recent works deal with the use of flux vector control to achieve MTPA this without the need for tables [20], [21].

The recent works discussed in the previous paragraph highlight the interest of making flux control laws for these motors, presenting strong nonlinearity. In this paper, the use of flux as state variable instead of current which allows to get rid of the notion of differential inductances. Moreover, it is shown that a feedback linearization strategy transforms the nonlinear

model into a linear one which facilitates the control design. To evaluate the new control law, it is important to propose and carry out realistic dynamic simulations. Another contribution of the paper focusses on the realization of dynamic simulation of SynRM to perform flux control from FEA based motor design. While FEA tools provide nonlinear flux versus current characteristics, dynamic simulations of these machines requires the inverse. This paper presents a methodology to perform MTPA flux control on a SynRM from FEA nonlinear map obtained using the simulation software Finite Element Method Magnetics (FEMM). This work is a first step towards a joint optimization of the motor and its control.

The paper is divided into 3 sections. Section II presents the article motivations. Section III is dedicated to the modelling strategy from FEA, including MTPA characteristics. The model is used in Section IV to illustrates the advantage of using flux dynamics coupled with nonlinear control to ensure good performance at all operating points.

II. Motivations

In this section, the dynamic model of the SynRM is presented and the practical problem that motivated our research is introduced. Figure 1 shows a schematic of the two-phase four poles SynRM used in this article. It is a 2 kW machine with maximum torque of 2 N.m.

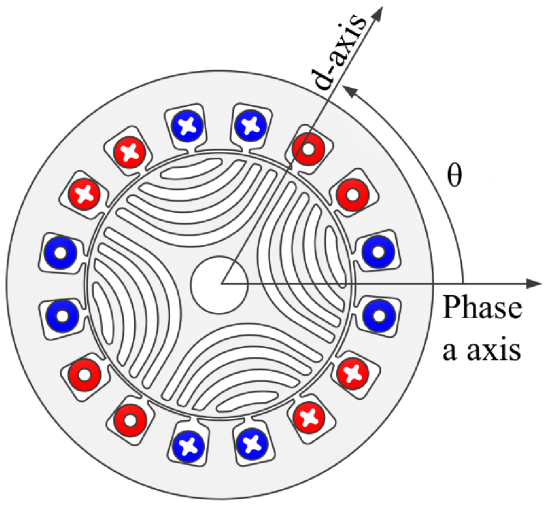

Fig. 1. Schematic of the SynRM.

Two-phase machine (and not a commonly used three-phase) means that voltages are applied to the motor in the two-phase stationary reference frame called $\alpha\beta$. The rotating reference dq-frame is obtained thanks to the Park rotation matrix defined as:

$$(\cdot)_{dq} = P(\theta)^{-1}(\cdot)_{\alpha\beta} \tag{1}$$

with

$$P(\theta) = \begin{bmatrix} \cos(p\theta) & -\sin(p\theta) \\ \sin(p\theta) & \cos(p\theta) \end{bmatrix},$$

where $\theta \in \mathbb{R}$ is the rotor mechanical angle and $p \in \mathbb{N}_+$ is the pole pairs number.

The dynamic of the windings in the dq reference frame is given by the state space system:

$$\dot{\lambda}_{dq}(t) = v_{dq}(t) - Ri_{dq}(t) - p\omega(t)\mathcal{J}\lambda_{dq}(t) \tag{2}$$

where $\lambda_{dq}(t) \in \mathbb{R}^2$ is the stator flux linkage, $v_{dq}(t) \in \mathbb{R}^2$ is the stator voltage, $i_{dq}(t) \in \mathbb{R}^2$ is the phase current and $\omega(t) \in \mathbb{R}$ is the rotor angular velocity. The matrix $R \in \mathbb{R}_+$ is the phase resistance diagonal matrix. The matrix $\mathcal{J}$ is a rotation matrix given by $\mathcal{J} = \begin{bmatrix}[0 & -1] & [1 & 0]\end{bmatrix}^\intercal$.

The flux-current dependence is a static nonlinear map, where the nonlinearity is introduced by saturation and cross-saturation [15], [22]. The apparent inductance is expressed as a nonlinear function $\ell_{dq}(i_{dq}) : \mathbb{R}^2 \to \mathbb{R}^2$ yielding to the model:

$$\lambda_{dq} = \ell_{dq}(i_{dq})i_{dq}. \tag{3}$$

Electric machines produce electromagnetic torque $\tau_{em} \in \mathbb{R}$ when the current interact with the magnetic field, i.e. flux. The torque equation is:

$$\tau_{em} = p\ i_{dq}^\intercal \mathcal{J}\lambda_{dq} \tag{4}$$

Remark. Note that for three-phase motors the produced torque in the dq frame is multiplied by a factor $3/2$ using Clarke transformation from three-phase abc to two-phase $\alpha\beta$ coordinates. ⌟

Usually, since current is measured, it is interesting to look at the dynamic of the current rather than the flux, from (2) one has:

$$\begin{aligned} &\left(\ell'_{dq}(i_{dq}(t))i_{dq}(t) + \ell_{dq}(i_{dq}(t))\right)\tfrac{di_{dq}(t)}{dt} = \\ &v_{dq}(t) - Ri_{dq}(t) - p\omega(t)\mathcal{J}\ell_{dq}(i_{dq}(t))i_{dq}(t). \end{aligned} \tag{5}$$

where the term $\ell'_{dq}(i_{dq})$ is referred as differential inductances. This adds complexity, pushing us to use the flux as a state variable (2).

On the other hand, the use of model (2) for simulation requires the knowledge of the current from the flux, The inversion of the nonlinear function $\ell_{dq}(i_{dq})$ is required:

$$i_{dq} = \lambda_{dq}^{-1}(\ell_{dq}(i_{dq})i_{dq}). \tag{6}$$

This article is dedicated to the flux dynamic modeling of a SynRM and the design of an MTPA based flux control based on data from FEA. The flux control allows the apply a simplified feedback linearization strategy and deal with linear flux equation only despite the nonlinearity (3). It highlights the usefulness of focusing on flux rather than current. The control objective is to produce the desired electromagnetic torque (4) from a reference torque $\tau^\#$, with the aim of minimizing Joule losses at steady state. It is equivalent to compute flux references $\lambda_{dq}^\#$ from $\tau^\#$.

III. Flux and MTPA characteristics from FEA

The mathematical dynamic model of the motor being introduced in the previous section, this section is dedicated to obtaining the nonlinear flux-current map (3) of the SynRM including magnetic saturation and cross-saturation obtained thanks to finite element analysis (FEA). To perform dynamic

simulation of the motor model, it is required to inverse the map given in equation (6), procedure detailed in this section. Finally MTPA trajectory is derived.

A. FEA analysis

The FEA is conducted using FEMM software on a single pole of the machine using Anti-Periodic and Air Gap boundary conditions [1]. Fig. 2 shows the geometry and the mesh used. The different materials are air and copper ($\mu = \mu_0$) and M-19 Steel which is a nonlinear laminated silicon iron soft magnetic material. The simulation has been run for different couple (I_s, γ) defined as follows:

$$I_s = ||i_{dq}|| \tag{7}$$

$$\gamma = \arg(i_{dq}) \tag{8}$$

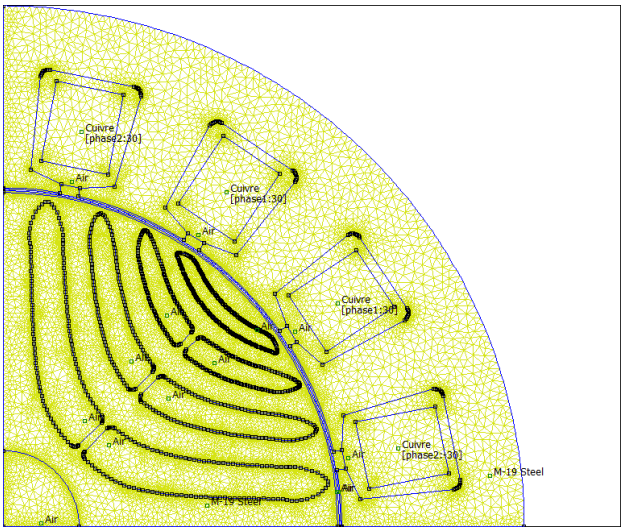

Fig. 2. Geometry and mesh of the FEA using FEMM software.

I_s and γ take each 10 values in the interval $[0 \quad 10]$ and $[0 \quad \pi/2]$ respectively, for a total of 100 combinations. For each combination, the simulation has been run for 10 mechanical positions of the rotor varying from 0 to 45 degree. This range of rotor positions is enough to capture a full period of the machine behavior. The FEA simulation then returns the average torque and average dq flux over the 10 mechanical positions for each (I_s, γ) combination equivalent to different (i_{dq}) combinations.

The nonlinear characteristics that links current to flux modelled equation (3) obtained from FEA are plotted Fig. 3.

To highlight the impact of cross-saturation, i.e., the impact of current i_k with $k \in d, q$ on λ_l for $l \neq k$, Fig. 4 represents the flux λ_{dq} for minimal and maximal current.

Remark. Fig. 4 clearly shows saturation at low current on q axis due to flux barrier while saturation on the d axis appear for higher current due to larger quantity of iron in this axis. ⌟

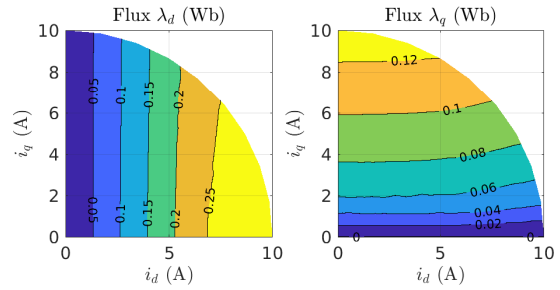

Fig. 3. Nonlinear flux-current characteristic obtained from FEMM.

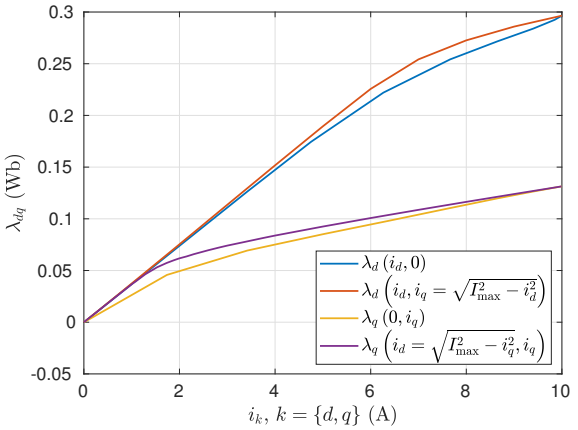

Fig. 4. Representation of the minimal and maximal flux λ_{dq} with respect to current.

B. Simulation model

From the previously obtained maps, simulation of the dynamic behavior of the motor flux modelled in (2) requires the inverse map given in equation (6) has represented on the simulation schematic given Fig 5.

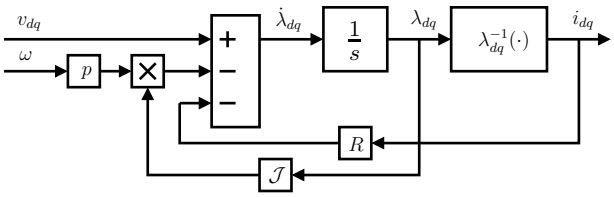

Fig. 5. Simulation model of the flux dynamics (2) .

The inversion has been obtained numerically using the Matlab function **fmincon** which finds minimum of constrained nonlinear multivariable functions. For each pair λ_{dq}, the objective was to find the pair i_{dq} which minimize the objective function:

$$\left[\lambda_{dq}^{\text{FEMM}} - \ell_{dq}(i_{dq})i_{dq}\right]^{\intercal} W \left[\lambda_{dq}^{\text{FEMM}} - \ell_{dq}(i_{dq})i_{dq}\right], \tag{9}$$

with $W = \text{diag}\left\{w_1^2, w_2^2\right\}$ and $w_2 = 3w_1$ in order to normalize the amplitudes factor of the different flux components λ_{dq} as represented Fig. 4. Multiple initial conditions were given to the optimization algorithm through a multi-start procedure to avoid local minima in the function. The results for the

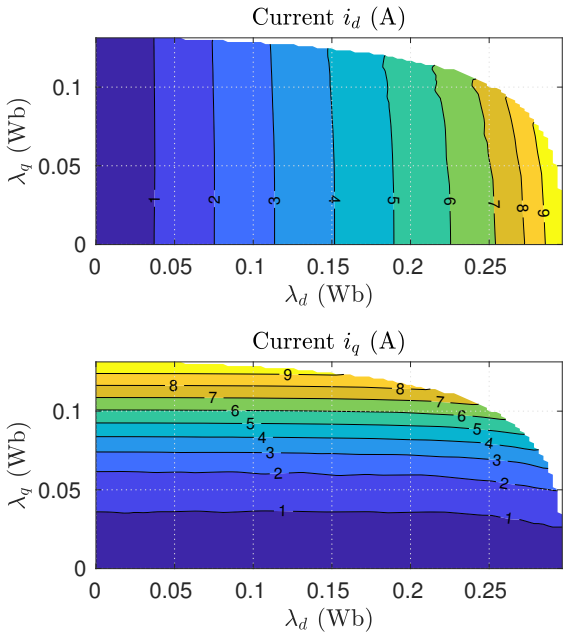

Fig. 6. Nonlinear current-flux characteristic obtained from numerical inversion.

nonlinear inversion is plotted on Fig. 6 For this simulation, the remaining parameters are $p = 2$, $R = 0.52\ \Omega$.

C. MTPA-LUT derivation

From the characteristics represented Fig. 3 and the electromagnetic torque given equation (4) one can obtain the torque-flux characteristic represented on Fig. 7. It illustrates the torque levels as a function of the flux which implies that a reference torque can be produced from an infinite combination of flux λ_{dq}. The figure also highlights the necessity of producing larger flux on the d axis than on the q axis to produce torque.

The MTPA objective is to minimize the Joules losses, given by:

$$P_{Joules} = Ri_{dq}^{\intercal} i_{dq}. \tag{10}$$

The criterion therefore consists in minimizing the norm of the current i_{dq} i.e. $||i_{dq}^{\star}||$ which are computed by minimizing the current magnitude. One poses:

$$i_{dq} = I_s \begin{bmatrix} \cos(\gamma) \\ \sin(\gamma) \end{bmatrix} \tag{11}$$

where I_s is the current magnitude and γ is the current angle [20]. The MTPA trajectory coincides with:

$$\frac{d\tau_{em}}{d\gamma} = 0, \tag{12}$$

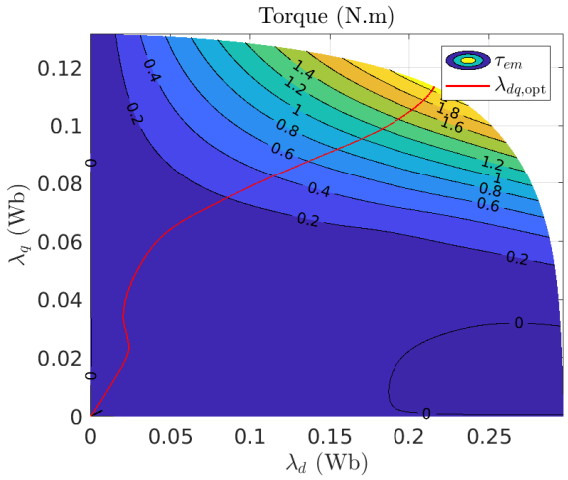

Fig. 7. Torque-flux characteristic and MTPA trajectory (red).

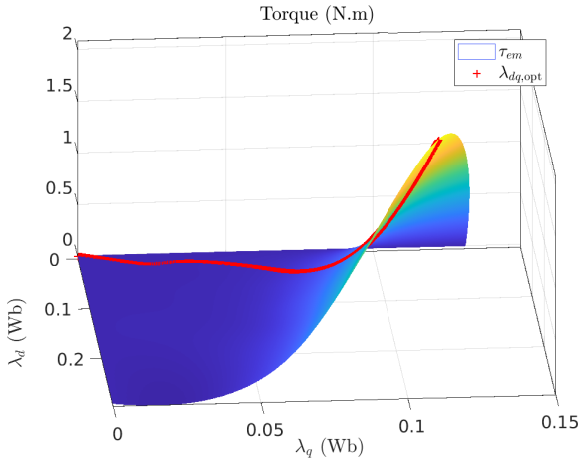

Fig. 8. Torque-flux characteristic and MTPA trajectory, obtained from FEMM.

which can be computed numerically from the LUT given Figure 7. The numerically computed MTPA is represented on the torque map Fig. 8. On the Fig. 9 representing the derivative of torque, MTPA corresponds, indeed to the bottom of the valley.

IV. LUT BASED FLUX CONTROLLER FOR MTPA

The flux control objective is the regulation of the flux with reference flux provided by the MTPA trajectory represented in red on Fig. 7. Note that, in spite of Park transformation, the flux model given equation (**??**) remains non-linear. However, having access to the current measurement, speed measurement and flux reconstruction from LUT, it is possible to apply a feedback linearization. The proposed control algorithm is thus composed by two parts, a feedback linearization to compensate the nonlinearities and a feedback control to impose the closed loop dynamic. Similar approach can be found applied to the current controller of a permanent magnet motor in [4]. Recent work proposes to do without LUTs [20], [21]. The overall

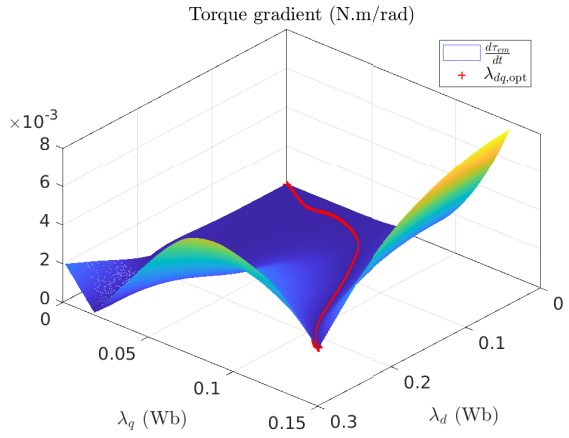

Fig. 9. The derivative of torque with respect to the current angle and the MTPA trajectory obtained with FEMM.

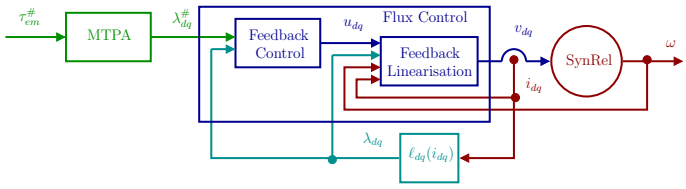

Fig. 10. Representation of the overall control scheme.

control scheme is represented Fig. 10. Note that the reference torque can be directly a torque reference or a reference computed from an outer speed control loop. This outer loop is out of the scope of this article.

a) Feedback linearization: Choosing

$$v_{dq} = u_{dq} + Ri_{dq} + p\omega\mathcal{J}\lambda_{dq}, \tag{13}$$

equation (2) with (13) becomes:

$$\dot{\lambda}_{dq} = u_{dq} \tag{14}$$

It results in a time invariant linear system, in which the fluxes λ_d and λ_q are independent, leading to pure integrator. This is why this linearization is often called "decoupling".

Remark. The equivalent feedback linearization applied on the current dynamic (5) would require much more complicated calculation to become linear. ⌟

b) Dynamic control: One of the control objectives is to ensure a zero static error, that is why an integral action is added in the feedforward path between the error comparator and the plant. This control strategy generally called type 1 Servo system, since the plant has no integrator [14, p. 743]. The two flux equations being independent, for $k \in \{d, q\}$, one has:

$$\varepsilon_k = \int (\lambda_k^{\#} - \lambda_k) d\tau, \tag{15}$$

the integrator output and then:

$$\begin{aligned} \dot{\lambda}_k &= u_k, \\ \dot{\varepsilon_k} &= \lambda_k^{\#} - \lambda_k, \end{aligned} \tag{16}$$

with the control:

$$u_k = -k_p\lambda_k - k_I\varepsilon_k, \tag{17}$$

with k_p and k_I the control gains to be tuned using Ackerman's formula to impose the dynamics described by a second order system with the classical characteristic polynomial equation

$$P(s) = s^2 + 2\zeta\omega_n s + \omega_n^2, \tag{18}$$

where, the parameters ω_n and ζ are the desired closed loop pulsation and damping coefficient.

The control objective is the obtaining of closed loop flux dynamic with 5% overshoot and time response equal to 3 ms leading to the characteristic polynomial given in (18) with $w_n = 100$ rad/s and $\zeta = 0.7$ and control gain $k_p = 140$ and $k_i = -10000$. The desired torque $\tau^{\#}$ is defined as a stair sequence for 0 to 1.8 Nm with a step of 0.2 Nm. Through the torque-flux characteristics, the flux reference is computed. The simulation are represented on Fig. 11. The figure shows that indeed, for regular torque steps, the flux steps amplitudes varies, highlighting the nonlinear nature of the system. However, 5% time response for the different amplitudes remains equal, as represented on Fig. 12 were the step response for each step response errors are superposed, validating the linear behavior of the closed loop system. Finally, the resulting flux and torque are reported on the torque-flux characteristic plotted on a new figure, Fig. 13, for clarity. The figure highlights again the performance of the proposed control strategy and shows that at steady state, the MTPA trajectory plotted in red is perfectly covered by the references and the controlled flux.

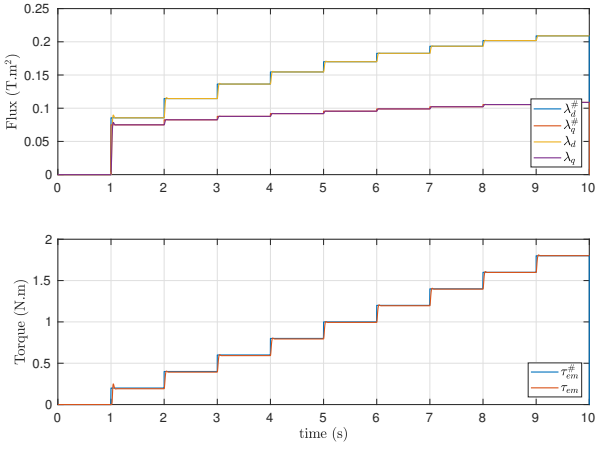

Fig. 11. Chronograph of the simulation results for the proposed approach.

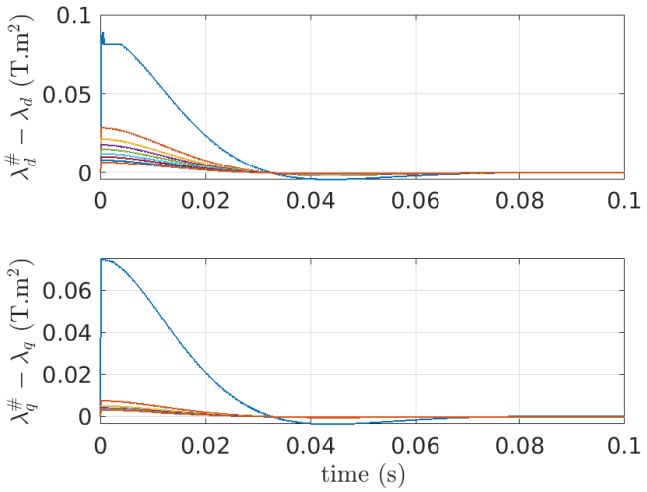

Fig. 12. Chronograph of the simulation errors for the proposed approach, each color representing a step of Fig. 11.

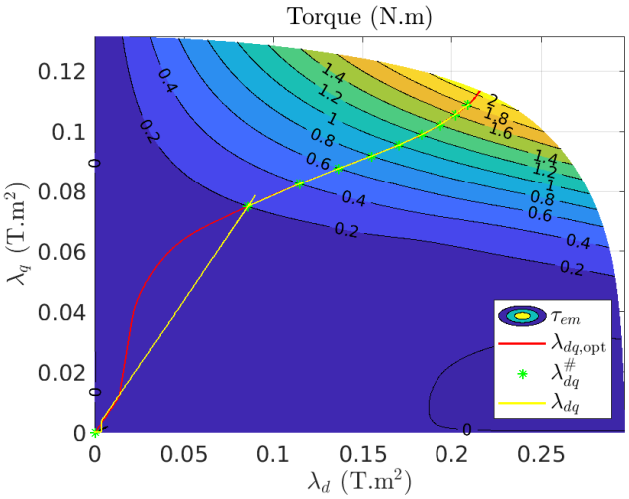

Fig. 13. Torque-flux characteristic, MTPA trajectory, reference and controlled flux.

V. Conclusion and Perspectives

In this article was studied the modelling of SynRM including magnetic saturation and cross-saturation to obtain accurate dynamic simulations from models obtained by FEA. It was shown that in the presence of nonlinear magnetic materials, the use of flux instead of current is of interest for both simulation and control design. From this observation, dynamic flux model was proposed and an MTPA based flux control developed. Simulation results, close to the real SynRM obtain from FEA validate our development and its practical usefulness.

As future work, real-world experiments are on the way to evaluate the gap between simulation and experimentation and validate the methodology under real conditions, including the inverter nonlinearities such as dead-time effect and switching device voltage drop among others. Theoretical developments are also underway to propose a flux observer that would make it possible to do away with LUTs.

References

[1] Rotor motion using an (anti)periodic air gap boundary condition. https://www.femm.info/wiki/RotorMotion. Accessed: 2023-02-22.

[2] B. Ban, S. Stipetić, and M. Klanac. Synchronous reluctance machines: Theory, design and the potential use in traction applications. pages 177–188, 2019.

[3] Y. Bao, M. Degano, S. Wang, L. Chuan, H. Zhang, Z. Xu, and C. Gerada. A novel concept of ribless synchronous reluctance motor for enhanced torque capability. *IEEE Transactions on Industrial Electronics*, 67:2553–2563, 2020.

[4] M. Bodson, J.-N. Chiasson, R.-T. Novotnak, and R.-B. Rekowski. High performance nonlinear feedback control of a permanent magnet stepper motor. *IEEE Transactions on Control Systems Technology*, 1:5–14, 1993.

[5] A. Boglietti and M. Pastorelli. Induction and synchronous reluctance motors comparison. pages 2041–2044, 2008.

[6] J. Bonifacio and R.-M. Kennel. On considering saturation and cross-coupling effects for copper loss minimization on highly anisotropic synchronous machines. *IEEE Transactions on Industry Applications*, 54(5):4177–4185, 2018.

[7] B. Cheng and T.-R. Tesch. Torque feedforward control technique for permanent-magnet synchronous motors. *IEEE Transactions on Industrial Electronics*, 57(3):969–974, 2010.

[8] C. M. Donaghy-Spargo. Synchronous reluctance motor technology : opportunities, challenges and future direction. *Engineering & technology reference.*, pages 1–15, May 2016.

[9] H. Ge, Y. Miao, B. Bilgin, B. Nahid-Mobarakeh, and A. Emadi. Speed range extended maximum torque per ampere control for pm drives considering inverter and motor nonlinearities. *IEEE Transactions on Power Electronics*, 32(9):7151–7159, 2017.

[10] H.-F. Hofmann, S.-R. Sanders, and A. EL-Antably. Stator-flux-oriented vector control of synchronous reluctance machines with maximized efficiency. *IEEE Transactions on Industrial Electronics*, 51(5):1066–1072, 2004.

[11] H. Kärkkäinen, L. Aarniovuori, M. Niemelä, J. Pyrhönen, and J. Kolehmainen. Technology comparison of induction motor and synchronous reluctance motor. pages 2207–2212, 2017.

[12] W. Lee, J. Kim, P. Jang, and K. Nam. On-line mtpa control method for synchronous reluctance motor. *IEEE Transactions on Industry Applications*, 58(1):356–364, 2022.

[13] U.S. Department of Energy. Critical materials strategy, 12 2011.

[14] K. Ogata. *Modern Control Engineering*. Prentice Hall, 2010.

[15] M. Preindl and S. Bolognani. Optimal state reference computation with constrained mtpa criterion for pm motor drives. *IEEE Transactions on Power Electronics*, 30(8):4524–4535, 2015.

[16] M.-A. Rahman. History of interior permanent magnet motors. *IEEE Industry Applications Magazine*, 19:10–15, 2013.

[17] A. Rassolkin, H. Heidari, A. Kallaste, T. Vaimann, J.-P. Acedo, and E. Romero-Cadaval. Efficiency map comparison of induction and synchronous reluctance motors. pages 1–4, 2019.

[18] F. Tinazzi, S. Bolognani, S. Calligaro, P. Kumar, R. Petrella, and M. Zigliotto. Classification and review of mtpa algorithms for synchronous reluctance and interior permanent magnet motor drives. In *2019 21st European Conference on Power Electronics and Applications (EPE '19 ECCE Europe)*, pages P.1–P.10, 2019.

[19] A. Vagati, M. Pastorelli, and G. Franceschini. High-performance control of synchronous reluctance motors. *IEEE Transactions on Industry Applications*, 33:983–991, 1997.

[20] A. Varatharajan, G. Pellegrino, and E. Armando. Direct flux vector control of synchronous motor drives: A small-signal model for optimal reference generation. *IEEE Transactions on Power Electronics*, 36(9):10526–10535, 2021.

[21] A. Varatharajan, G. Pellegrino, and E. Armando. Direct flux vector control of synchronous motor drives: Accurate decoupled control with online adaptive maximum torque per ampere and maximum torque per volts evaluation. *IEEE Transactions on Industrial Electronics*, 69(2):1235–1243, 2022.

[22] T.-G. Woo, S.-W. Park, S.-C. Choi, H.-J. Lee, and Y.-D. Yoon. Flux saturation model including cross saturation for synchronous reluctance machines and its identification method at standstill. *IEEE Transactions on Industrial Electronics*, 70(3):2318–2328, 2023.